Direct Growth Rate Measurement of Hydroxyapatite Single Crystal by Moire Phase Shift Interferometry

Noriko Kanzaki,[†] Kazuo Onuma,*[,‡] Atsuo Ito,[‡] Kay Teraoka,[†] Tetsuya Tateishi,[‡] and Sadao Tsutsumi[†]

Institute of Earth Science, School of Education, Waseda University, 1-6-1 Nishiwaseda, Shinjuku-ku, Tokyo, 169-0051 Japan, and National Institute for Advanced Interdisciplinary Research, 1-1-4 Higashi, Tsukuba, Ibaraki, 305-8562 Japan

Received: March 16, 1998; In Final Form: June 9, 1998

The growth rate of the hydroxyapatite (0001) face in pseudophysiological solution was measured directly for the first time by Moire phase shift interferometry. Common-path-type interferometry and a newly developed signal processor used for the phase shift technique enabled the precise and stable measurement of growth rates. It was determined that the growth rate was strongly time-dependent. The growth rate gradually decreased with time and finally ceased although the concentration of the solution remained constant. The thickness of the layer grown on the seed crystal was about 500−700 nm, while the growth rate during initial growth stages was of the order of 10^{-2} nm/s. respectively. Detailed surface morphology was observed by atomic force microscopy (AFM), indicating that the growth mode was multiple two-dimensional nucleation.

1. Introduction

Hydroxyapatite [$Ca_{10}(PO_4)_6(OH)_2$, HAP] is the major inorganic component of human bones and teeth and has been utilized as a representative bioactive material. It is important to clarify the growth mechanism of HAP not only to obtain conclusive information about the biomineralization process in vivo but also for the development of more bioactive implants. Although many studies have been performed to reveal the growth mechanism of HAP under physiological conditions, details of the growth mechanism of HAP are still unclear. The main reason for this is that all previous works were based on indirect methods. In the case of growth rate measurement, the growth rates of HAP were estimated from the weight change of precipitated HAP polycrystal, component and pH changes of the solution, etc.[1−5] The growth rate obtained by these indirect methods was the average of the growth rates of many crystals and every face of these crystals. Conclusive information about the growth mechanism can be obtained from direct growth rate measurement for each surface of the crystal combined with the surface observation.

We succeeded in synthesizing large HAP single crystals by means of the hydrothermal technique, and direct investigation of the growth kinetics for each crystal face was possible. Using these synthesized crystals as the seeds, Onuma et al. first reported the growth kinetics of HAP ($10\bar{1}0$), *a*-face, under pseudophysiological conditions by in situ atomic force microscopy (AFM). It was observed that the *a*-face grew by step flow combined with two-dimensional nucleation and the rate-determining process of the growth was found to be the incorporation of a growth unit at the step front, from the measurement of step velocities.[6] The growth rate of the *a*-face was estimated to be of the order of 10^{-4} nm/s from the step advancing rate. This value is about 3−4 orders of magnitude smaller than those for soluble inorganic crystals.

In contrast, the growth kinetics of HAP (0001), *c*-face, remain unclear. It should be important to elucidate the growth kinetics of the *c*-face, because HAP growth is elongated in the [0001] direction in bone matrix and in tooth enamel. The aim of this study is, thus, to investigate the growth kinetics of the HAP *c*-face under pseudophysiological conditions. Special attention is paid to measuring the growth rate of the *c*-face by the newly developed interferometric technique, and the growth mechanism of the HAP *c*-face is discussed, taking into account the results of AFM surface observation and X-ray photoelectron spectroscopy (XPS) analysis.

2. Experimental Section

2.1. Synthesis of HAP Seed Crystal. HAP single crystals were grown by the hydrolysis of monetite ($CaHPO_4$) according to the reaction process shown in eq 1 by the hydrothermal technique:

$$10CaHPO_4 + 2H_2O \rightarrow Ca_{10}(PO_4)_6(OH)_2 + 4H_3PO_4 \quad (1)$$

Large-grained $CaHPO_4$, about 1 μm in size, was prepared by dissolving four-nine grade calcium carbonate powder into extra-pure reagent orthophosphoric acid solution at pH 2 and 100 °C. The thermal and pressure conditions of the synthesis were about 260 °C and 150 kg/cm^2, respectively. The detailed procedure of the synthesis is given in ref 7. Synthesized HAP belongs to a hexagonal system with lattice constants $a = 0.9435$ nm and $c = 0.6882$ nm. The grown crystal has a needle-shaped morphology elongated in the [0001] direction bounded by ($10\bar{1}0$) and (0001) faces. The typical size of the seed crystal used for the present study is 1−2 mm in length and 20−40 μm in width.

2.2. Solution for HAP Growth. The pseudophysiological solution used for this study contains 140 mM NaCl, 2.5 mM $CaCl_2$ and 1 mM $K_2HPO_4 \cdot 3H_2O$ buffered at pH 7.4 by tris-(hydroxymethyl)aminomethane and 1 N HCl. All reagents were extra-pure grade and ultrapure sterile water was used. Before the addition of any reagent, the water was boiled and bubbled

* To whom correspondence should be addressed: Tel. +81-298-54-2557; Fax +81-298-54-2565; E-mail onuma@nair.go.jp.
† Waseda University.
‡ National Institute for Advanced Interdisciplinary Research.

S1089-5647(98)01512-0 CCC: $15.00
Published on Web 07/31/1998

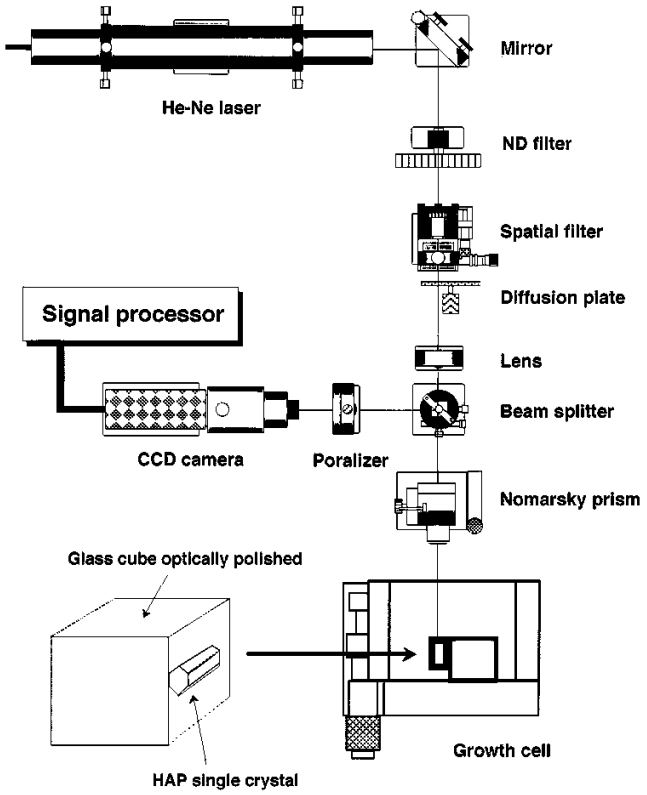

Figure 1. Schematic diagram of common-path-type interferometry using a Nomarsky prism. HAP single crystal glued on the glass cube is set in the growth cell filled with the pseudophysiological solution.

with N_2 gas for 30 min to remove all dissolved CO_2 gas. The growth temperature was constant at 25 °C.

2.3. Interferometry. A schematic diagram of the interferometry used for this study is shown in Figure 1. As the growth rate of the HAP *c*-face is assumed to be 2−3 orders of magnitude smaller than those of other inorganic crystals, precise and stable growth rate measurement is required. Common-path-type interferometry using a Nomarsky prism was employed to eliminate disturbances originating from mechanical vibrations, temperature fluctuations etc., instead of normal two-beam interferometry such as Michelson-type interferometry, which is highly sensitive to disturbance, and has been used for growth rate measurements of inorganic crystals by several researchers.[8−11]

The inlet polarized laser light beam is split into *p*- and *s*-waves by the Nomarsky prism with shearing of about 50 μm. Each light beam creates an image of the crystal surface separated from each other by 50 μm and interference takes place where the two images are overlapped. As the optical paths of *p*- and *s*-waves are almost the same, a stable interferogram against disturbance can be created. As the interference fringe corresponds to the three-dimensional profile difference between the two images, continuous movement of the fringes due to surface growth will be canceled when the interference takes place between the same crystal surface. We thus prepared the sample as follows. The HAP seed crystal is glued on the glass cube (7 mm × 7 mm × 7 mm), whose surfaces are optically polished. The crystal is glued on one side of the glass cube and the *c*-face is placed at the same level as the optically polished glass surface, which is schematically shown in Figure 1. Owing to the small crystal size as compared to the amount of shearing, 50 μm, the interference takes place between the glass surface and the *c*-face, which enables us to pursue the continuous movement of the fringes resulting from the growth of the *c*-face.

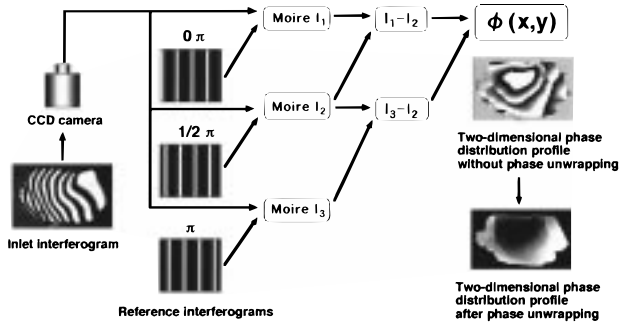

Figure 2. Signal process of Moire phase shift interferometry. The calculation process of a two-dimensional phase distribution profile of the *c*-face from an inlet interferogram is schematically shown.

Zero-thermal-expansion glass (Clearcerum Z, Ohara Co. Ltd.) for the growth cell, special magnetic ball-bearing stages (PI Polytic Co. Ltd.) that eliminate the backlash of the mechanical movement of the cell, and the Nomarsky prism were also employed. The interferometry was placed in a thermostated room with temperature fluctuation ± 1 °C.

A real-time phase shift technique is suitable for precise measurement of the three-dimensional height profile of the crystal surface.[12−16] The conventional real-time phase shift technique requires three inlet interferograms with a phase difference of $\pi/2$ with respect to each other to reconstruct the three-dimensional surface profile.[15] Three charge-coupled device (CCD) cameras with three polarizers were used for this purpose; however, phase error and mismatch of the images of the crystal surface between the three cameras occurs, which become severe in the case of extremely small sized crystals as in the present study. To overcome these problems, the Moire phase shift technique with one CCD camera was employed using the newly developed signal processor as described in the following section.[17]

2.4. Signal Processor. The signal processing procedure is shown in Figure 2. One interferogram of HAP *c*-face is input into the CCD camera. The intensity of the inlet interferogram I is expressed by eq 2, which includes information for the two-dimensional phase distribution profile, $\phi(x,y)$, of HAP *c*-face:

$$I = a(x,y) + b(x,y)\cos[2\pi x/P + \phi(x,y)] \qquad (2)$$

where $a(x,y)$, $b(x,y)$, and P are the bias, amplitude, and pitch, respectively.

As three unknown parameters are included in eq 2, three interferograms with different phases are necessary to calculate the two-dimensional phase distribution profile, $\phi(x,y)$. To calculate $\phi(x,y)$, three reference interferograms with a phase difference of $\pi/2$ with respect to each other are digitally composed in the signal processor as the carrier fringes. The reference interferograms have vertical equidistant fringes whose number is variable according to the inlet interferogram. Three Moire interferograms Ij ($j = 1, 2, 3$) are created between the inlet interferogram of HAP *c*-face and three reference interferograms in the signal processor. Three Moire interferograms Ij ($j = 1, 2, 3$) also have phase differences of $\pi/2$ with respect to each other, which are expressed in

$$I_1 = G(x,y) + Q(x,y)\cos\phi(x,y) \qquad (3)$$

$$I_2 = G(x,y) - Q(x,y)\sin\phi(x,y) \qquad (4)$$

$$I_3 = G(x,y) - Q(x,y)\cos\phi(x,y) \qquad (5)$$

where $G(x,y)$ and $Q(x,y)$ are the bias and amplitude, respectively.

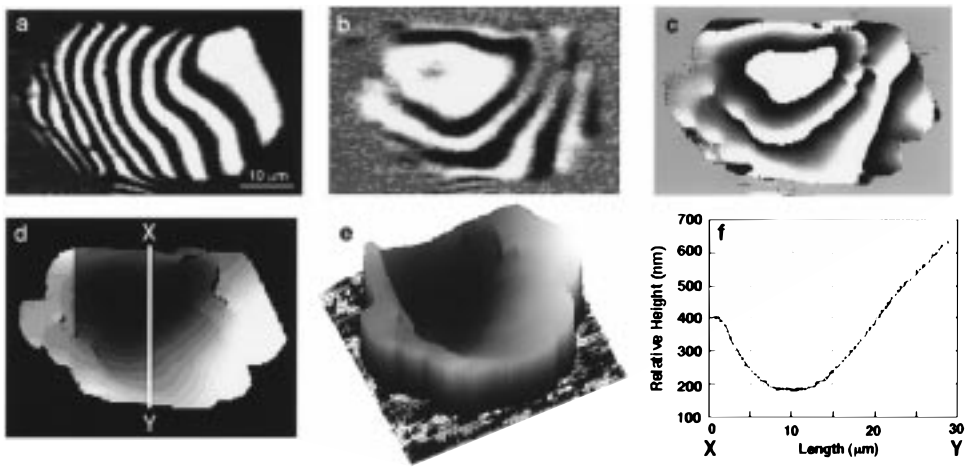

Figure 3. Example of the observation of the HAP *c*-face by Moire phase shift interferometry. (a) An inlet interferogram. (b) Moire interferogram corresponding to I_1-I_2. (c) Two-dimensional phase distribution profile without phase unwrapping. (d) Two-dimensional phase distribution profile after phase unwrapping. (e) Three-dimensional surface profile. (f) Section profile of line X−Y in panel d.

After creation of Moire interferograms, the inlet interferogram and the reference interferograms are completely subtracted by a digital filter in the signal processor. The two-dimensional phase distribution profile $\phi(x,y)$ is calculated by using eqs 3−5 as

$$\phi(x,y) = \tan^{-1}[(I_3 - I_2)/(I_1 - I_2) + \pi/4] \qquad (6)$$

$\phi(x,y)$ is shown as a gray-level picture whose color changes from black to white at each 2π interval. The signal processor uses a 9-bit digital value for the phase data and the color is exhibited as a digit in the range 0−511. As $\phi(x,y)$ is discontinuous at each 2π interval, phase unwrapping is necessary to reconstruct a perfect two-dimensional phase distribution profile of the crystal surface. Details of the unwrapping technique can be seen in ref 18. All the processes are finished in TV rate, $^1/_{30}$ s, by the new signal processor.

As the two-dimensional phase distribution profile after unwrapping is proportional to the three-dimensional height profile, $h(x,y)$, as shown in eqs 7 and 8, the three-dimensional height profile change, Δh, with time at each point of the crystal surface can be monitored by the change of the phase value, Δp, and the growth rate is measured:

$$\phi(x,y) = h(x,y)4\pi n/\lambda \qquad (7)$$

$$\Delta h = (2\pi\Delta p/512)(\lambda/4\pi n) \qquad (8)$$

where n is the refractive index of the solution, 1.33, and λ is the laser wavelength, 632.8 nm. The theoretical minimum height resolution is about 0.5 nm for the present interferometry.

2.5. Atomic Force Microscopy. NanoScope III-a AFM (Digital Instruments Inc.) with the tapping mode was employed to observe the detailed morphology of the HAP *c*-face grown in the pseudophysiological solution. The crystals were dipped in the solution and retrieved after 10 min, 2 h, and 24 h of growth, respectively. The surface morphologies were observed and compared with those before dipping. Silicon cantilevers with the spring constant 20−50 N/m and J-type (100 μm scanning range) piezo scanners were used for all the observations.

2.6. X-ray Photoelectron Spectroscopy. The layers grown on the seed surfaces were analyzed by XPS using a Quantum-2000 spectrometer (Physical Electronics Inc.) with an AlKα X-ray source ($h\nu$ = 1486.6 eV). As the pseudophysiological solution used for the present experiment is supersaturated for both HAP and octacalcium phosphate [$Ca_8H_2(PO_4)_6{\cdot}5H_2O$, OCP], the Ca/P ratios of the grown layers were measured for characterization of the materials. The diameter of the X-ray beam was about 20 μm, smaller than the size of the *c*-face, and the pressure in the spectrometer was about 3×10^{-9} Torr. The analyzer pass energy was 187.85 eV for qualitative analysis and 58.70 eV for quantitative analysis. An Ar^+ shower was employed to compensate the charge valence with an electron shower used for preventing the accumulation of positive charges on the surface. After AFM observation, the samples were used for XPS analysis, and all the samples were preserved under N_2 gas atmosphere to avoid CO_2 adsorption until the XPS measurement.

3. Results

3.1. Observation by Moire Phase Shift Interferometry. An example of HAP *c*-face observation by the present Moire phase shift interferometry is shown in Figure 3. Panel a is an original inlet interferogram, panel b is a Moire interferogram corresponding to $I_1 - I_2$ in eq 6, panel c is a two-dimensional phase distribution profile without phase unwrapping, and panel d is a two-dimensional phase distribution profile after phase unwrapping. Relative phase difference on the surface is displayed with a color change from black to white in each 2π as shown in panel c. By phase unwrapping, the discontinuous points in panel c are connected and a perfect two-dimensional phase distribution profile with smooth color change is obtained as seen in panel d. As the two-dimensional phase distribution profile can be converted to the three-dimensional height profile according to eq 7, the surface morphology is reconstructed as seen in panel e. The section profile along the x−y line is shown in Figure 3f, indicating that the surface takes a hopper morphology and the height difference between the center and edge positions is about 400 nm. All the processes mentioned here are finished in TV rate, $^1/_{30}$ s, in the signal processor. The values of two-dimensional phase distribution profiles of the surface are recorded at desired time intervals and the phase value change with time at each point of the crystal surface is monitored. The relative height change at each point is calculated from the phase value change, according to eq 8.

3.2. Growth Rate Measurement. Figure 4 is the result of growth rate measurement of the HAP *c*-face. Figure 4a shows the relationship between time and relative height measured at the center of the surface. It is found that the relative height does not exhibit linear increase with time; that is, the growth

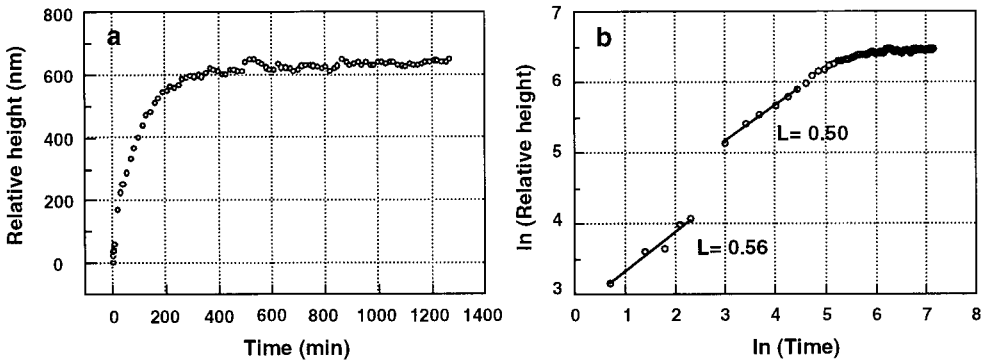

Figure 4. (a) Relative height vs time on the HAP *c*-face. Note that the growth rate shows strong time dependence. The growth rate gradually decreases with time and finally stops. (b) Ln (relative height) vs ln (time) on the HAP *c*-face. Note that the slopes are 0.50 and 0.56, indicating that the diffusion process for growth is strong at the initial stage.

rate is not constant and is strongly time-dependent. The relative height quickly increases at the beginning of growth, indicating that the growth rate is high at the initial stage. However, the relative height increase rate becomes slow and the growth rate gradually decreases with time and finally the growth stops after about 7 h. The total thickness of the newly grown layer is about 600 nm as seen in Figure 4a. The range of total thickness of the grown layer caused by different kinds of seed crystals is 500−700 nm. As the growth rate is not constant, we defined the growth rate at the beginning of the growth. The measured data are fitted by a simple polynomial function and the growth rate is calculated from the slope of tangent to the curve at the time $t = 0$. The growth rate of the HAP *c*-face under the present condition was found to be about 8×10^{-2} nm/s, which is 2 orders of magnitude larger than that of the HAP *a*-face. All measurements showed the same growth rate versus time characteristics, and no remarkable difference between different kinds of seed crystals and the measured points in the same crystal was observed. The fluctuation of measured data, $\pm$ 20 nm, is found after growth stopped, which is due to unavoidable thermal expansion and contraction of metal stages used for interferometry resulting from temperature fluctuations in the room.

To estimate the effect of diffusion resistance on growth, the relationship between ln (time) and ln (relative height) is presented in Figure 4b. During the first 2 h, the data are fitted by a straight line except at 10−20 min, where the growth rate increase is temporary. The slopes of the two lines are 0.50 and 0.56.

3.3. AFM Observation. The detailed surface morphologies of the grown crystals are observed by AFM as seen in Figure 5. Panel a is the seed crystal surface and panels b−d are the surface morphologies after 10 min, 2 h, and 24 h of growth, respectively. After the crystals were dipped in the solution, the surfaces were covered with two-dimensional islands indicating that the growth mode of the *c*-face was multiple two-dimensional nucleation. The sizes of the two-dimensional islands after 10 min, 2 h, and 24 h of growth were 10−20 nm, 20−30 nm, and 30−40 nm, respectively. Three-dimensional coalesced islands, 200 nm in size, are also seen after 24 h of growth. The average island size increases until 2 h of growth; however, it is constant after 24 h of growth.

3.4. XPS Analysis. The seed crystal and the grown layers obtained after 10 min, 2 h, and 24 h of growth are analyzed by XPS. Addition of apatitic elements (Ca, P, O) and C and Si on the seed surface and on all the grown layers are detected and in particular, Na is detected on all the grown layers as shown in Figure 6.

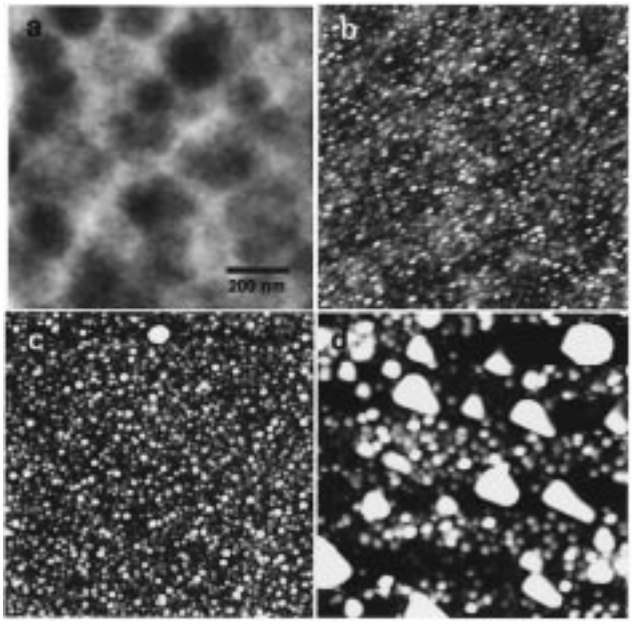

Figure 5. AFM images of the HAP *c*-face. (a) Seed surface. (b) Surface after 10 min of growth. (c) Surface after 2 h of growth. (d) Surface after 24 h of growth in the pseudophysiological solution.

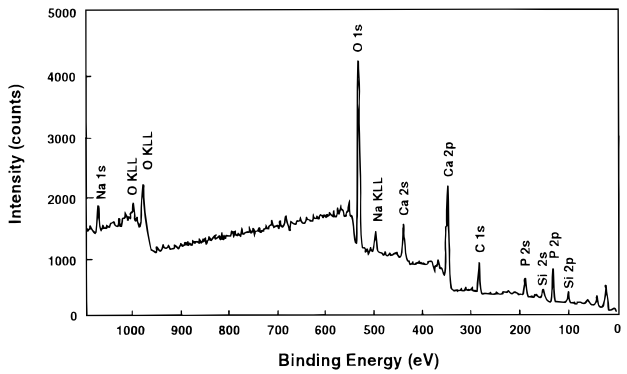

Figure 6. XPS wide-scan spectrum of the HAP *c*-face after 10 min of growth in the pseudophysiological solution.

The results of the quantitative analysis and the Ca/P ratios for the seed and the grown layers are given in Table 1. All the Ca/P ratios after correction, Ca/P*, are larger than 1.50 for the grown layers, indicating that Ca-deficient HAP grows under the present condition. The Ca/P* ratio is the highest in the seed, 1.66, and gradually increases for the grown layer with the dipping time in the solution. Ca2p3/2, P2p, O1s, and C1s peaks are used for quantitative analysis. These Ca/P* ratios were

TABLE 1: Relative Concentration of the Elements and the Ca/P Ratio Detected on HAP *c*-Face[a]

dipping time	relative concentration (atomic %)					
	O	C	Ca	P	Ca/P	Ca/P*
seed surface	41.1	38.9	11.4	8.6	1.33	1.66
10 min	55.6	18.6	14.0	11.8	1.19	1.50
2 h	41.7	43.2	8.4	6.8	1.24	1.56
24 h	46.1	37.0	9.4	7.5	1.25	1.58

[a] Ca/P* indicates the corrected value by using the Ca/P ratio of the seed crystal, 1.66.

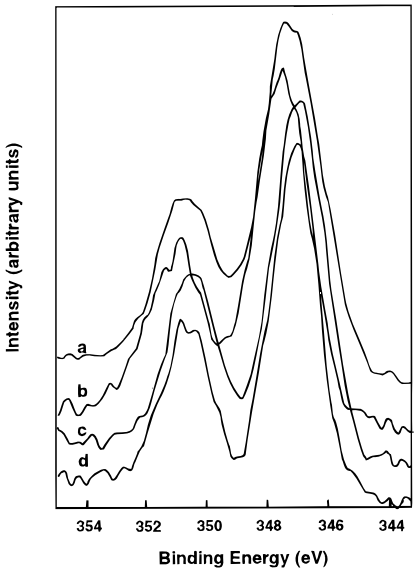

Figure 7. Ca 2p peaks of the HAP *c*-face. (a) Surface after 10 min of growth. (b) Surface after 2 h of growth. (c) Surface after 24 h of growth in the pseudophysiological solution. (d) Seed surface.

corrected by using the ratio of the seed crystal (Ca/P = 1.66), measured by inductively coupled plasma (ICP) spectrometry.

The crystallinity of the grown layer increases with dipping time as seen from the Ca 2p spectra in Figure 7 and the peak shape of the sample after 24 h of growth is similar to that of the seed surface.

4. Discussion

The growth mode of the HAP *c*-face has been considered as spiral growth in some previous reports; however, the direct surface observation by AFM revealed that the growth proceeded with multiple two-dimensional nucleation mode.[1−3]

It is found by XPS analysis that the layers grown on the seed crystals are Ca-deficient HAP, although OCP is considered as the precursor of HAP under physiological conditions.[19] However, Boskey and Posner[20] reported that HAP grew directly under lower supersaturation, and it is observed that Ca-deficient HAP grew directly also under the present study. The increase of the crystallinity and the Ca/P ratio of the grown layer with dipping time indicates the maturation phenomenon. In the present study, the Ca/P ratio of the seed surface is 1.33, although the Ca/P ratio of HAP single crystals measured by ICP is 1.66−1.67. In the case of the grown layers, the Ca/P ratios are 1.19−1.25. Anderson and Kangasniemi[21] have reported that the Ca/P ratio of Ca-deficient HAP measured by XPS analysis was 1.0−1.3.

The C1s peak at 285.0 eV detected on the seed surface and on all the grown layers can be attributed to carbon contamination reported by Santos et al.[22] Moreover, a large shoulder near 286.0 eV is observed on the layer grown for 2 h and a small shoulder near 286.0 eV is seen on the layer grown for 24 h, which is considered to correspond to the C−O bond of tris-(hydroxymethyl)aminomethane as the buffer in the solution. The O1s peak of the layer grown for 2 h is shifted to a higher binding energy as compared with the other samples This may also indicate that the C−O bond near 532−533 eV attributed to tris-(hydroxymethyl)aminomethane, exists more on the layer grown for 2 h than on other samples.

Si detected on the seed surface is attributed to silica glass tube used for the synthesis of the HAP single crystal and Si detected on the grown layers is attributed to the sterile water used for the solution. Na is attributed to NaCl used for the solution and is considered to substitute the Ca site in the HAP structure.

The direct crystal growth rate measurement of the HAP *c*-face was followed by Moire shift interferometry. The growth rate of the *c*-face is 1 or 2 orders of magnitude larger than that of the *a*-face. This result agrees with the morphology of the HAP single crystal, which is elongated in the [0001] direction. From the results of the growth rate measurements as seen in Figure 4a, it is found that the growth rate of the HAP *c*-face shows time dependence. The decrease in the degree of supersaturation of the solution during the growth process is usually considered to be the reason behind the time-dependent growth rate. The quantitative analysis of the solution by ICP indicates no difference in the concentration of Ca and P between before growth (Ca, 101.7 ppm; P, 32.1 ppm) and after growth (Ca, 101.2 ppm; P, 32.1 ppm) was observed. Arens et al.[4] also reported the time dependence of the HAP growth rate and concluded that the growth rate decrease with time was attributed to the surface maturation phenomenon, as a result of which the number of available growth sites decreases. The maturation phenomenon is actually observed by XPS analysis in this study. However, in the case of this study, the growth stopped completely, which is different from the case of Arens et al. Thus, some other factors should be considered, such as the following: (1) The impurity effect of Si or tris(hydroxymethyl)-aminomethane in the solution. XPS analysis shows the possibility of adsorption of tris(hydroxymethyl)aminomethane and Si on the grown layers. These elements cannot substitute the HAP structure, and may inhibit growth through physical adsorption on the surface. To confirm the impurity effect, the growth rate was measured in the solution using half the concentration of tris(hydroxymethyl)aminomethane, the lowest limit required to maintain the pH of the solution as 7.4. However, the result was the same as that in the solution with normal tris(hydroxymethyl)aminomethane concentration (the data is not shown here). In this case, the amount of tris-(hydroxymethyl)aminomethane is still much larger as compared with other reagents such as Ca and P; thus, growth rate measurements in the solution without tris(hydroxymethyl)-aminomethane are necessary in future studies to confirm the impurity effect of tris(hydroxymethyl)aminomethane. The concentration of Si is so small that a method to eliminate Si from the solution has not yet been developed. (2) Strain accumulation between the seed and the grown layer during the growth. XPS analysis shows that the crystallinity of the grown layers is low as compared with that of the seed surface, and the chemical compositions of the grown layers are different from that of the seed crystal. In this case, strain is caused by lattice misfit produced at the interface between the seed surface and the grown layer. The strain energy, ΔE, increases the chemical potential of the crystal, $\mu_{crystal}$. The driving force for the growth, the chamical potential difference, $\Delta\mu$, is expressed by

$$\Delta\mu = \mu_{\text{solution}} - \mu_{\text{crystal}} \tag{9}$$

In the case that strain exists, $\Delta\mu$ is expressed by eq 10 and it relatively decreases.

$$\Delta\mu = \mu_{\text{solution}} - (\mu_{\text{crystal}} + \Delta E) \tag{10}$$

As ΔE increases with the thickness of the grown layer unless misfit dislocation is introduced, $\Delta\mu$ becomes extremely small and the growth almost stops despite the supersaturation of the solution. (3) The electric potential change develops on the crystal surface during the growth. From a previous study of the HAP *a*-face as mentioned in the Introduction, the Posner cluster,[23] $Ca_9(PO_4)_6$, is considered to be the growth unit of HAP crystal growth.[24] The cluster is thought to have a positive charge caused by Ca^{2+} located outside the cluster, although the total charge is neutral. In the case that the cluster is the growth unit of the HAP *c*-face, the positive charge is accumulated during cluster stacking on the seed surface. An electric repulsion is produced between the crystal surface and clusters incorporated into the crystal and the growth stops.

The logarithmic plot between the relative height and the time shows that the slope of the line is 0.50−0.56, indicating that the volume diffusion process for growth is strong during the initial stage of growth. This result seems to conflict with the result of the previous study for the HAP *a*-face in which the rate-determining process of the growth was found to be the incorporation of a growth unit at the step front. However, if the $Ca_9(PO_4)_6$ cluster is the growth unit, it is considered that a strong bond site exists in the [0001] direction and there is no strong bond site in the $[10\bar{1}0]$ direction as shown in ref 25. The incorporation process is thus easier in the [0001] direction than in the $[10\bar{1}0]$ direction, which makes the rate-determining process between *c*- and *a*-faces different.

5. Conclusion

The direct crystal growth rate measurement of the HAP *c*-face was accomplished by interferometry. Common-path-type interferometry used with Moire phase shift technique is the most suitable method for slow growth rate measurement.

Acknowledgment. We thank Dr. K. Tukamoto of Tohoku University for rent of the Nomarsky prism.

References and Notes

(1) Moreno, E. C.; Zahradnik, R. T.; Glazman, A.; Hwu, R. *Calcif. Tissue Res.* **1977**, *24*, 47.
(2) Koutsoukous, P.; Amjad, Z.; Tomson, M. B.; Nancollas, G. H. *J. Am. Chem. Soc.* **1980**, *102*, 1553.
(3) Moreno, E. C.; Varughese, K. *J. Cryst. Growth* **1981**, *53*, 20.
(4) Arends, J.; Christoffersen, J.; Christoffersen, M. R.; Eckert, H.; Fowler, B. O.; Heughebaert, J. C.; Nancollas, G. H.; Yesinowski, J. P.; Zawacki, S. J. *J. Cryst. Growth* **1987**, *84*, 515.
(5) Christoffersen, M. R.; Cristoffersen, J. *J. Cryst. Growth* **1992**, *121*, 617.
(6) Onuma, K.; Ito, A.; Tateishi, T.; Kameyama, T. *J. Cryst. Growth* **1995**, *154*, 118.
(7) Ito, A.; Nakamura, S.; Aoki, H.; Akao, M.; Teraoka, K.; Tsutsumi, S.; Onuma, K.; Tateishi, T. *J. Cryst. Growth* **1996**, *163*, 311.
(8) Chernov, A. A.: Kuznetsov, Yu. G.: Smol'skii, I. L.: Rozhanskii, V. N. *Sov. Phys. Crystallogr.* **1986**, *31*, 705.
(9) Chernov, A. A.: Rashkovich, L. N. *J. Cryst. Growth* **1987**, *84*, 389.
(10) Onuma, K.; Tsukamoto, K.; Sunagawa, I. *J. Cryst. Growth* **1990**, *100*, 125.
(11) Maiwa, K.; Tsukamoto, K.; Sunagawa, I. *J. Cryst. Growth* **1990**, *102*, 43.
(12) Bruning, J. H.; Herriot, D. R.; Gallagher, J. E.; Rosenfeld, D. P.; White, A. D.; Brangaccio, D. J. *Appl. Opt.* **1974**, *13*, 2693.
(13) Nakadate, S.; Yamaguchi, I. Japanese patent laid-open H02-287107, 1990.
(14) Onuma, K.; Tsukamoto, K.; Nakadate, S. *J. Cryst. Growth* **1993**, *129*, 706.
(15) Onuma, K.; Kameyama, T.; Tsukamoto, K. *J. Cryst. Growth* **1994**, *137*, 610.
(16) Onuma, K. *Jpn. J. Microgravity Appl.* **1995**, *13* (3), 188.
(17) Shibata, T.; Nakamura, T.; Kuwashima, S. *O. Plus E.* **1996**, *202*, 101.
(18) Onuma, K.; Nakamura, T.; Kuwashima, S. *J. Cryst. Growth* **1996**, *167*, 387.
(19) Brown, W. E.; Eidelman, N.; Tomazic, B *Adv. Dent. Res.* **1987**, *1*, 306.
(20) Boskey, A. L.; Posner, A. S. *J. Phys. Chem.* **1976**, *80*, 40.
(21) Anderson, O. H.; Kangasniemi, I. *J. Biomed. Master. Res.* **1991**, *25*, 1019.
(22) Santos, J. D.; Jha, L. J.; Monteiro, F. J. *J. Mater. Sci. Mater. Med.* **1996**, *7*, 181.
(23) Posner, A. S.; Betts, F. *Acc. Chem. Res.* **1975**, *8*, 273.
(24) Onuma, K.; Ito, A.; Tateishi, T. *J. Cryst. Growth* **1996**, *167*, 773.
(25) Onuma, K.; Ito, A. Submitted to *Chem. Mater.*